CHAPTER 4

RESULTS AND DISCUSSION

This chapter shows the results of experimental and discussion. Phase formation and chemical composition analysis, microstructure of GST material, mechanical properties and thermoelectric properties.

Sample Preparation

The polycrystalline sample of GST was bought from rare-metal material company, China. The cylindrical ingots sample had dimensions of 38.15 x 5.018 mm^2. The sample called GST-hotpress company.

Figure 27 Shows a Germanium antimony telluride ingot from rare-metal material company, China and dimensions of cylindrical ingot

Phase Formation

Thermogravimetry and Differential Thermal Analysis

The behavior of melting temperature of GST–hotpress company sample analyzed by using TG–DTA were performed on ∼10 mg of sample sealed inside evacuated aluminum oxide (Al_2O_3) container. The sample was heated from room temperature to 1273 K with a heating/cooling rate of 293 K/min, as shown in Figure 27 It can see that the temperature of about 423–723 K in blue line TG%, the weight of GST–hotpress company sample has decreased with increasing temperature, corresponding to Tellurium has evaporation of the starting materials. In the green line, DTA has decreased by melting in two steps of in the weight loss at each temperature. First drop consist by Tellurium has evaporation occur, which in this part is endothermic effect of Tellurium. The second drop occurs in the temperature above 880 K consists a melting point from this part indicating relative of TG% and DTA because in this part the weight of GST–hotpress company compound have decreased to zero value with increasing temperature. The reaction described the system of GST–hotpress company absorbs energy from surrounding in measurement; usually but not always in the form of heat.

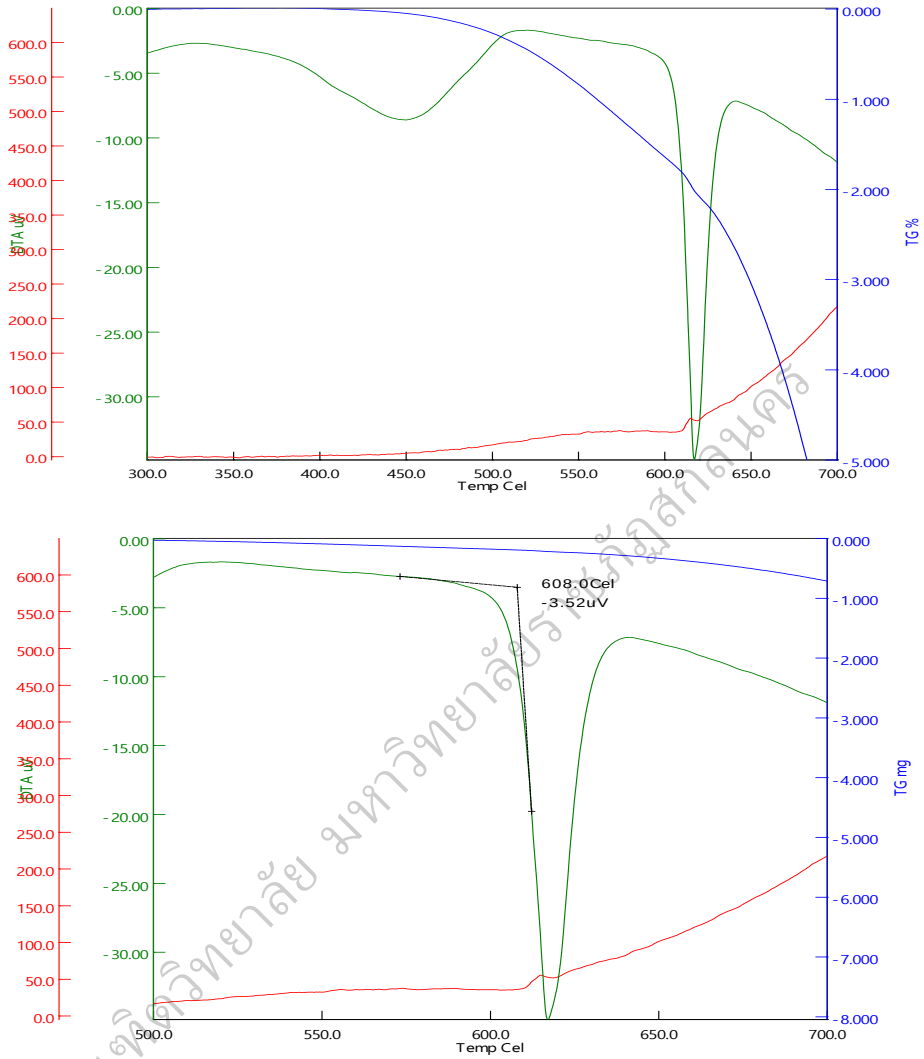

Figure 28 The TG and DTA vs temperature of GST-hotpress company sample (a) evaporation of Te showing at 673 K (b) the melting temperature of GST-Hotpress company showing at 873 K.

Energy Dispersive X-ray Spectroscopy

The elemental compositions of the sample were determined using energy-dispersive X-ray spectroscopy (EDX) at room temperature at an accelerating voltage of 15 keV on a Field Emission Scanning Electron Microscopy SU8000 (FE-SEM).

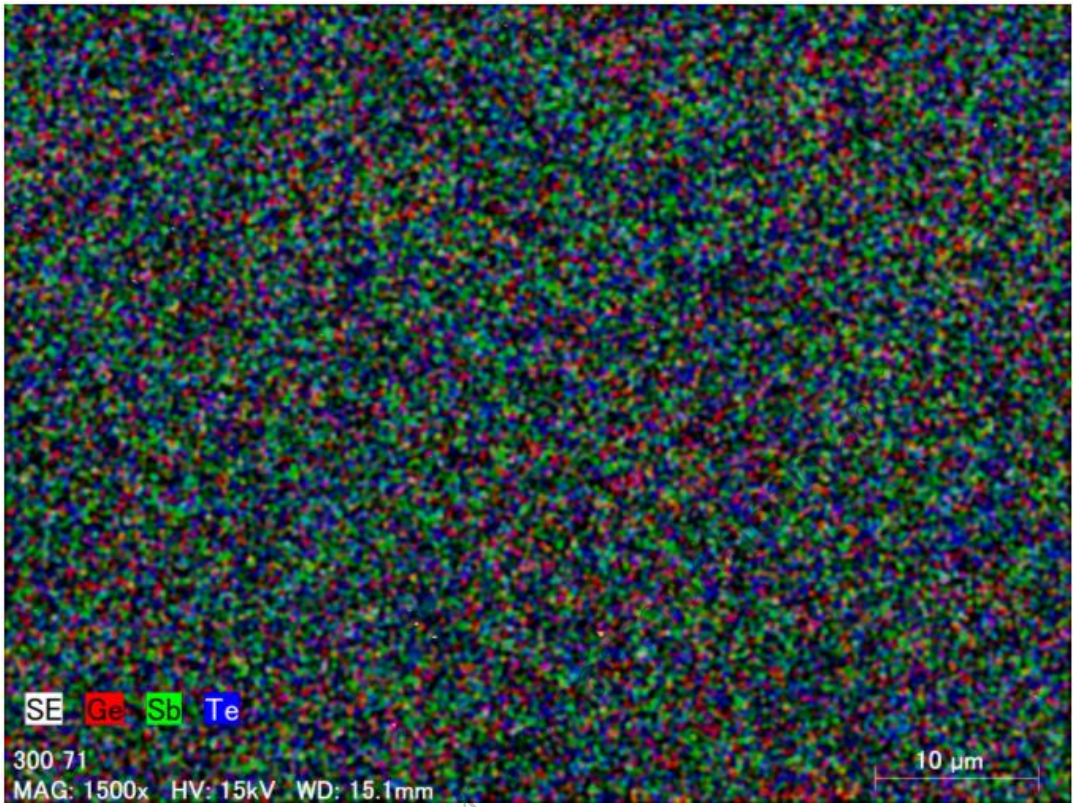

Figure 29 shows elemental mapping of GST-hotpress company, indicating apparent Ge deviation

In figure 4.4 show EDX mapping of GST-hotpress company sample. We was measured this area compare with another area (green circle). Yellow area is a $GeSb_6Te_{10}$ compound but in green circle is a Sb_2Te_3 compound. Therefore, from XRD results XRD found the patterns has a compound Sb_2Te_3 structure and $GeSb_6Te_{10}$ mixture in hot-pressed sample corresponding with EDX.

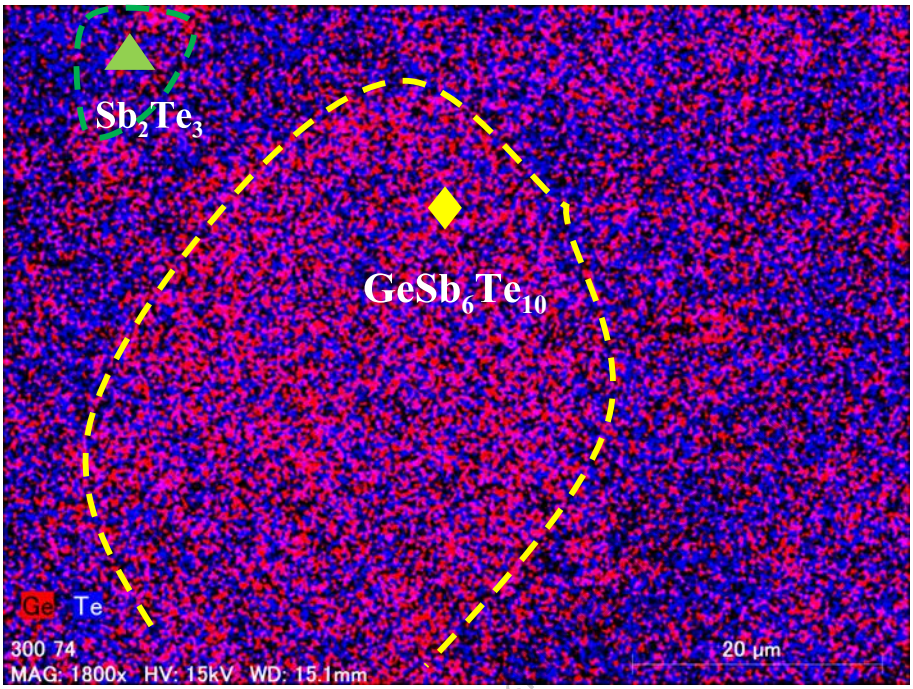

Figure 30 Shows EDX mapping by yellow circle we found grained were detected in GST-hotpress company sample

In these figure shows elemental mapping of GST-hotpress company sample, indicating apparent Ge-deviation. To investigate the spatial distribution of each element, we performed compositional analyses of GST-hot press at 50 randomly selected points within the surface area of ca. 52 × 76 μm^2 and the summarized the obtained results in Table 1 shows elemental compositions (%) of GST-hotpress company, GST-anneal, and GST-melt from literature (Kosuga et al., 2015).

	GST–hotpress company	GST–anneal	GST–melt	Nominal Composition
Ge	4.66±1.95	5.19±1.6	5.89±0.42	5.88
Sb	36.33±1.49	38.56±0.82	39.65±0.44	35.29
Te	59.00±0.96	56.25±1.1	56.46±0.58	58.82

In table 1, we found that the average composition of each element in GST–hotpress Company was slightly different from that of GST–melt and GST–anneal. This is probably attributed to the difference in composition between original GST ingot supplied for hot–pressing (GST–hotpress company), and for measurement as it is (GST–melt) and spark plasma sintering (GST–anneal). The samples of GST–melt and GST–anneal were prepared by us throughout all the preparation process and the preparation method of the GST ingot was the totally same for these samples, whereas the sample of GST–hotpress company was purchased from a company and perhaps the preparation condition of the ingot might be different from the rest of two samples. Therefore, this could cause a difference in the average composition of all elements between GST–hotpress sample, and GST–melt and GST–anneal. Therefore, we will not perform further discussion about it. Rather than the average composition, we predicted that the difference in the standard deviation of each element would reflect the process of hotpress, SPS, and without both. From Table 1, not only elemental Ge, but also Sb and Te in GST–hotpress as well as those of GST–SPS had larger standard deviation from those of GST–melt. The main difference between GST–hotpress company and GST–SPS, and GST–melt during the preparation process is that as for GST–hotpress company and GST–SPS, pressure and heat were

applied for the powder in order to fabricate sintered bulk materials, while GST–melt has no such kinds of treatment against the ingot. At this stage, the reason why this kind of compositional deviation occur is unclear. One of the possible explanation is, in the microscopic view point, a small extent of spatial inhomogeneity of pressure and heat during the sinter process is possible, thus the partial remelting and redistribution of the elements might occur in GST–hotpress company and GST–SPS. From the elemental compositional analysis at each point, we found that the there is a certain tendency in the ratio of Ge, Sb, and Te. For instance, Point A (Ge: Sb: Te=6.82, 35.52, 57.67) has close value of the nominal composition of GeSb6Te10 (Ge: Sb : Te =5.88, 35.29, 58.82). Whereas Point B (Ge: Sb: Te =8.64, 33.78, 57.58) has higher content of Ge and lower content of Sb than that of nominal composition. Likewise, Point C (Ge: Sb: Te=0.46, 40.79, 58.75) has lower content of Ge and higher ratio of Sb, than that of nominal composition.

Crystal Structure and Chemical Composition of GST

Crystal Structure and Grain Orientation

The X–ray diffraction (XRD) measurements was performed on Rigaku Smart Lab by using Cu–Kα1 radiation the angle from 3° to 90° at room temperature (λ = 1.5406 Å) as shown in Figure 31.

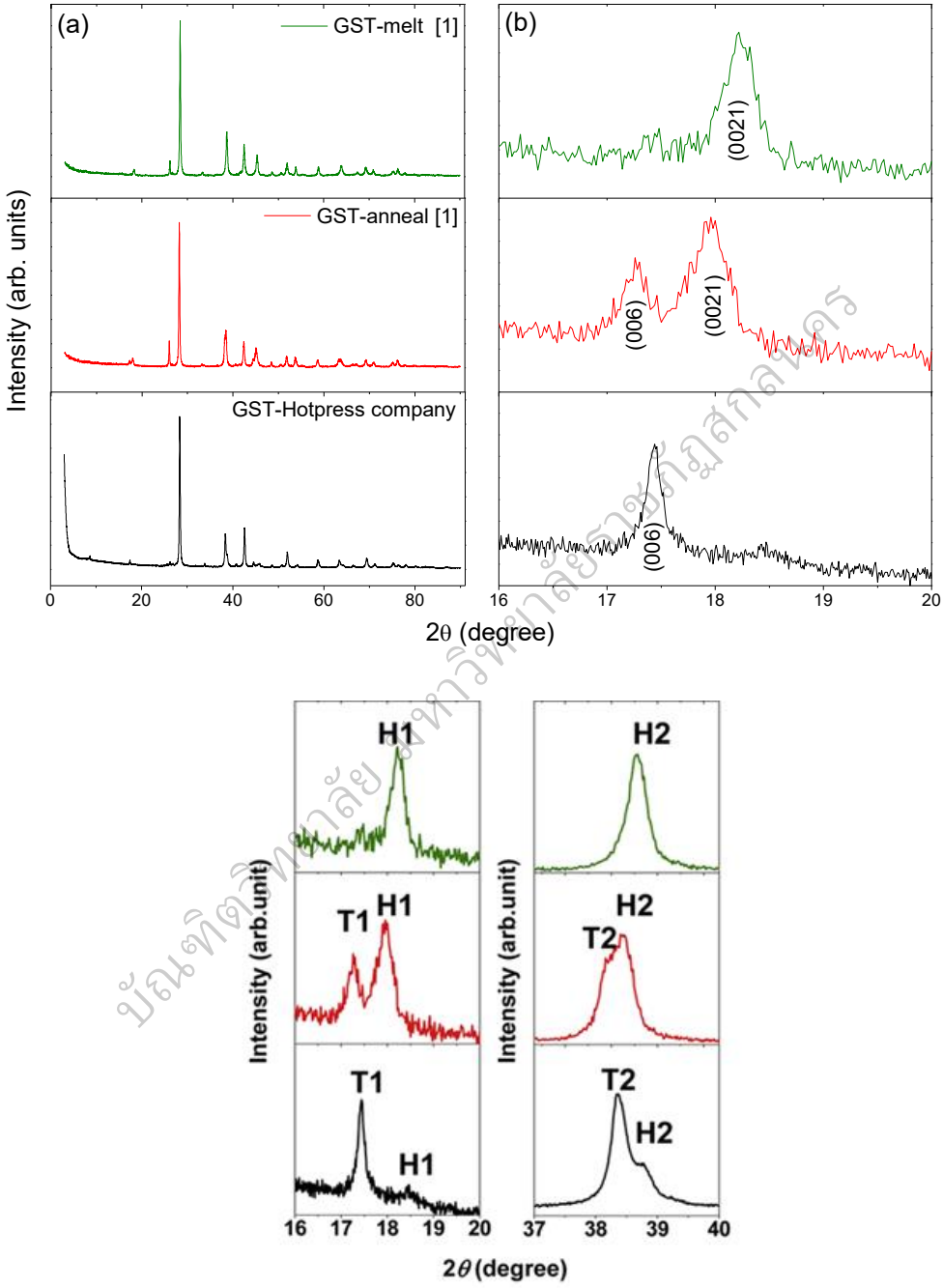

Figure 31 (a) XRD patterns of GST-hotpress company, GST-melt (Kosuga et al., 2014), and GST-anneal (Matsunaga et al., 2010). (b) Enlarged images in the range

2θ=16–20°. The left peak corresponds to the Bragg peak of the 0 0 6 tetradymite structure (denoted T1) and the right peak is that of the 0 0 21 homologous structure (denotedH1). (c) Enlarged images of the range 2θ=37–40°.The left peak corresponds to the Bragg peak of the 1010 tetradymite structure (denotedT2) and the right peak is that of the 1034 homologous structure (denotedH2).

Figure 31 the sample was identified diffraction peaks being from a single phase mixture of two types consisted of a $GeSb_6Te_{10}$– type homologous and Sb_2Te_3–type tetradymite structure (Kosuga et al., 2014). The Figure 31 shows the XRD pattern of GST–hotpress, together with those of GST–melt and GST–anneal (Kosuga et al., 2015). GST–melt and GST–anneal are polycrystalline samples of $GeSb_6Te_{10}$ prepared by melting and by SPS and subsequent annealing, respectively. The overall XRD pattern of GST–hotpress company is quite similar to those of GST–melt and GST anneal. However, there is an obvious difference in the range2θ=16–20° (Fig. 31(b)). In this range, GST–melt has a single peak corresponding to 0021_{HG} (HG represents a Bragg peak of the $GeSb_6Te_{10}$–type homologous structure), whereas GST–anneal has a new satellite peak corresponding to 006_{TD} (TD represents a Bragg peak of the Sb_2Te_3–type tetradymite structure) at the lower–angle side of 0011_{HG}. For GST–hotpress company, the intensity of the 006_{TD} peak is higher than that of the 0021_{HG} peak. Other peaks in different angle ranges show the same tendency (a typical example is shown in Fig. 31(c)). Based on this finding, we performed Rietveld analysis assuming that GST–hotpress company contains the $GeSb_6Te_{10}$–type HG structure and the Sb_2Te_3–type TD structure, and the data fitted well to a previously reported model. The obtained phase fraction ratio of the $GeSb_6Te_{10}$ structure to the Sb_2Te_3 structure is ca. 40–60wt.%. These results indicate that GST–hotpress company contains

not only the $GeSb_6Te_{10}$ structure but also the Sb_2Te_3 structure. The GST has been crystal structure of is hexagonal and high intensity in (hkl) of (0017) obtained the lattice parameters of a=4.26168, b=4.26168, c=101.73 (a=b≠c). It appeared that, where all the observed lines can be correspond 95%.

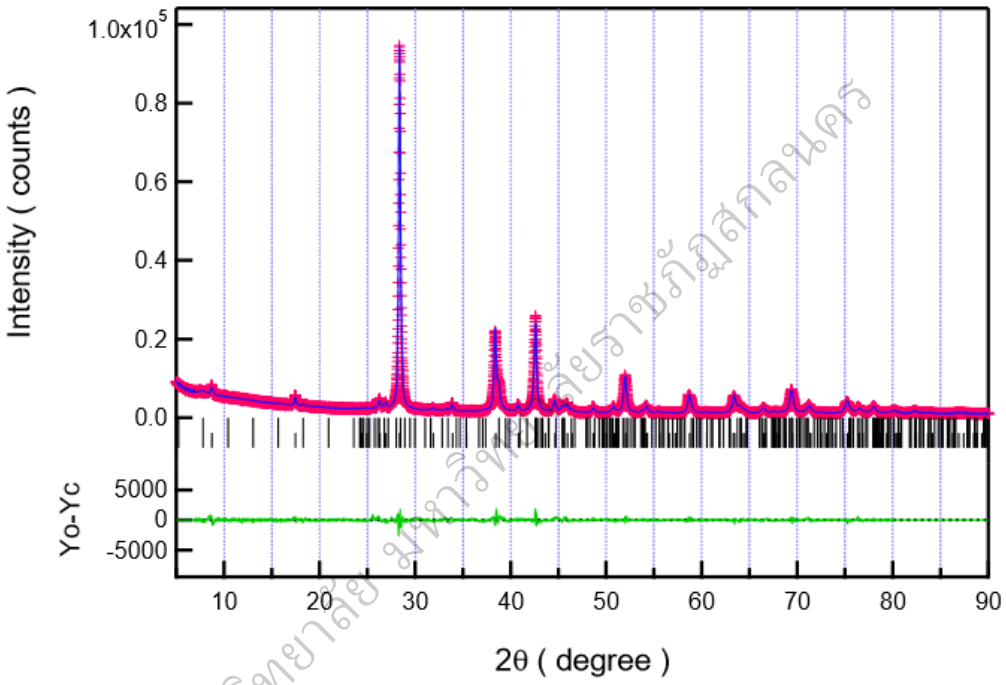

Figure 32 XRD patterns and Rietveld refinement of GST of GST–hotpress company. The dotted and solid lines represent the observed data and pattern fit, respectively. The vertical marks show the Bragg peaks of $GeSb_6Te_{10}$ with a homologous structure. The bottom curve was obtained the difference between the observed and calculated patterns (Namhongsa, Omoto, Fujii, Seetawan, & Kosuga, 2017)

Table 2 Room–temperature lattice parameters (*a* and *c*), lattice volume (*V*), and *R* factors (R_p and R_{wp}) of GST prepared by hotpressing method from company. The lattice parameter *a* and *c* were determined by Le Bail analysis.

	R_p	R_{wp}	*a*(Å)	*b*(Å)	*c*(Å)	*V*(Å^3)
$GeSb_6Te_{10}$(HP company)			4.2456	4.2456	101.6257	1587.0
Sb_2Te_3 (HP company)	2.92	3.81	4.2270	4.2270	30.4180	472.5
$GeSb_6Te_{10}$ (Matsunaga et al., 2010)	0.041	0.057	4.2360	4.2360	101.5087	1577.38
Sb_2Te_3 (Karpinsky, Shelimova, Kretova, & Fleurial, 1998) (Schneider & Oeckler, 2010)			4.2640	4.2640	30.4580	

The orientation degree of the (0 0 *l*) planes can be determined by the orientation factor *F*, which can be calculated using the Lotgering method (Lotgering, 1959):

$$F = \left(P - P_0\right) / \left(1 - P_0\right), \tag{4.1}$$

$$P = I\left(0\ 0\ l\right) / \sum I\left(h\ k\ l\right), \tag{4.2}$$

$$P_0 = I_0\left(0\ 0\ l\right) / \sum I_0\left(h\ k\ l\right), \tag{4.3}$$

where P and P_0 are the ratios of the integrated intensities of all (0 0 *l*) planes for the preferentially oriented and randomly oriented samples, respectively (Fan et al., 2006). The orientation factors *F* of the (0 0 *l*) planes of the sample with different direction between upper side and lower side of GST sample. The orientation factors of upper side have value about 0.31 but in lower side have an orientation factor approximately 0.255, indicating that the direction for pressing process has effect on arrangement in crystal structure of compounds. The orientation factor, *F* is equal to 1 for a perfect *c*–plane preferred orientation structure. The particles with upper side bonded by Van der Waals force would rotate perpendicular to the pressing direction. Thus, it was found that a lowest oriented GST sample.

Microstructure of GST-Hotpress Sample

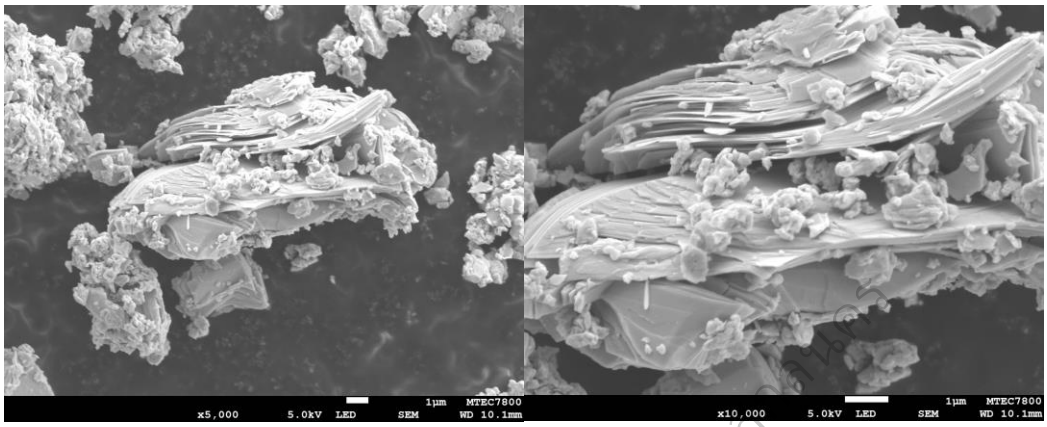

Figure 33 SEM images for GST particles prepared by a hot-pressing method (bar = 1 μm)

In the figure 33, GST-hotpress company shows exhibit denser microstructure after water quenched. From this grain of samples show that a distinct layer structure with the sheet of Sb_2Te_3, consistent with the hexagonal structure. On the slab of Sb_2Te_3 consist with Ge

Vickers Hardness

The Vickers hardness (H_V) was measured by micro hardness tester. The applied loads of 0.3 HV with loading time of 10 s. The H_V values of the GST-hotpress company sample was measured at room temperature and average from 3 indentations for a given sample. The average value of GST-hotpress company sample has ≈231.67 HV.

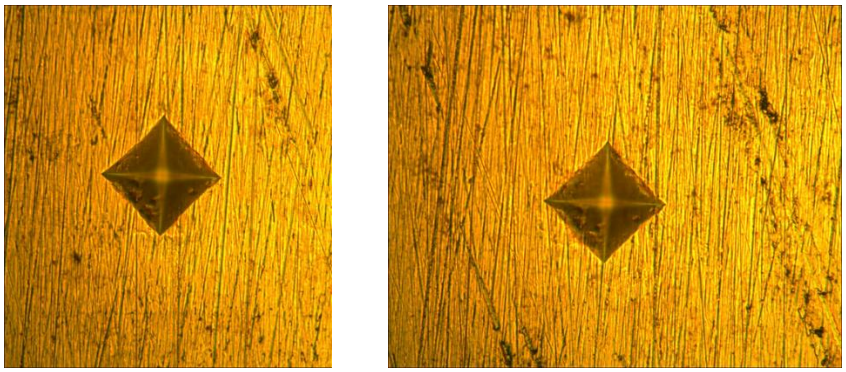

Figure 34 Shows pressing of GST–hotpress company sample from the micro hardness tester.

Thermoelectric Properties of GST–Hotpress Samples

Electrical Conductivity and Seebeck Coefficient values

In figure 35 shows the temperature dependence of the electric conductivity (ρ) of the GST–hotpress company sample, together with the literature data from Kosuga et al., 2015, temperature range 300 K – 723 K. The electrical conductivity of all the samples exhibits metallic conduction behavior and decreased with increasing temperature, which possibly results from the heavy degenerate nature of the compound semiconductor. The ρ values of the GST–hotpress company sample are 0.208 $M\Omega^{-1}$ m^{-1} at 310 K to 0.0965 $M\Omega^{-1}$ m^{-1} at 664 K respectively. The GST–hotpress company shows the same tendency as GST–melt and GST–anneal, but the values are slightly different. These values are lower than that of the GST–melt and GST–anneal samples of Kosuga *et al.* 0.241 $M\Omega^{-1}$ m^{-1} and 0.551 $M\Omega^{-1}$ m^{-1} respectively, which was prepared by spark plasma sintering.

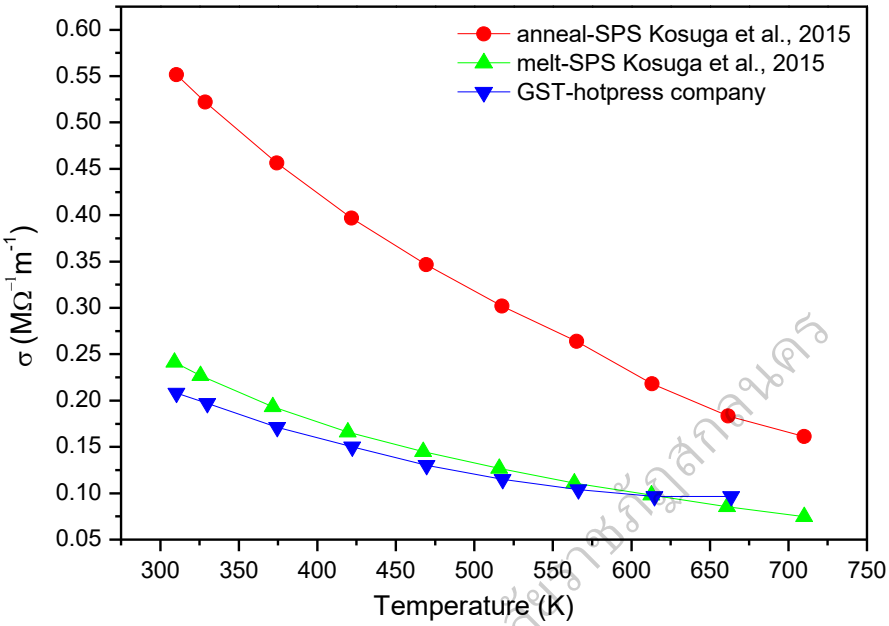

Figure 35 Show comparison the temperature dependence of the electrical conductivity of the GST–hotpress company sample with literature data [Kosuga *et al.*, 2015] (Namhongsa et al., 2017)

Figure 36 shows the temperature dependence of the Seebeck coefficient (S) of the GST–hotpress company sample compared with literature data. The S were measured in the temperature range of 300 – 723 K. The S values of these samples are positively, indicating p–type conduction. The S values of GST–hotpress company was increases with increasing temperature from 17.9μV K^{-1} at 310 K to 67.8μV K^{-1} at 664 K, respectively. However, these values are lower than that of the samples of Kosuga et al., but GST–hotpress company has Seebeck coefficient value similar like GST–anneal. Nonetheless, we observed at 573 – 673 K of GST–melt and GST–hotpress company were decreased a slightly caused of adjust behavior for into semiconductor type.

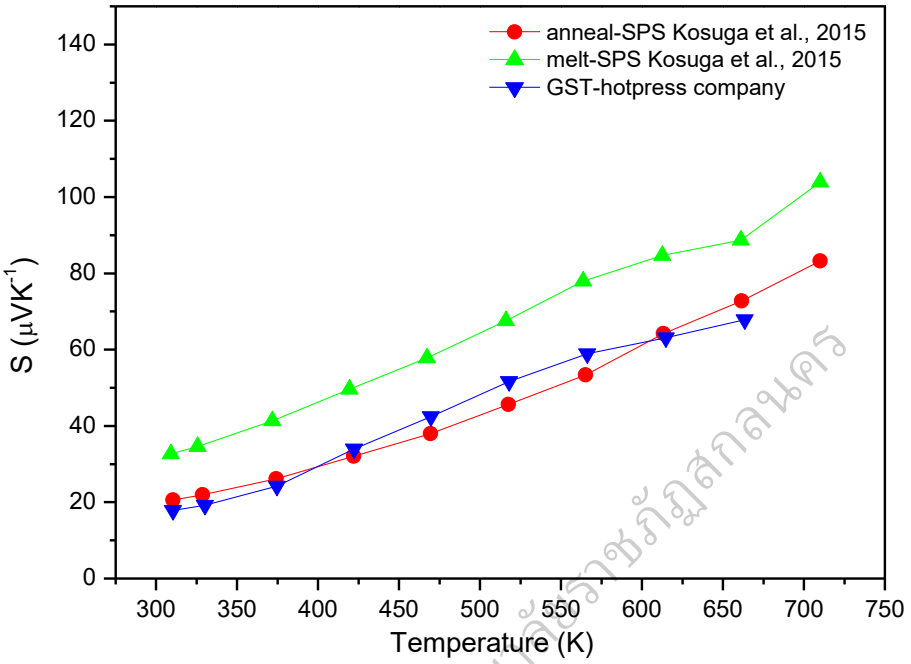

Figure 36 Show comparison the temperature dependence of the Seebeck coefficient of GST–hotpress company sample with literature data [Kosuga *et al.*, 2015] (Namhongsa et al., 2017)

Thermal Conductivity

Figure 37 shows the temperature dependence of the thermal conductivity (κ) of the GST–hotpress company sample compared with literature data. The thermal conductivity (κ) was calculated followed by equation:

$$\kappa = DC_p d \qquad (4\text{–}5)$$

Where D, C_p and d are the thermal diffusivity, specific heat capacity, and density of the ingot, respectively.

The κ values of these samples decreased with increasing temperature, The κ values of the GST-hotpress company were be similar to GST-anneal from literature data. The κ values GST-hotpress company sample is 3.4 $Wm^{-1} K^{-1}$, 2.48 $Wm^{-1} K^{-1}$ at 300 K, 623 K, respectively. However, the thermal conductivity of GST-hotpress company values have higher than that of literature data. Nonetheless, the thermal conductivity values of all have lower than that other semiconductor its means GST materials have a good thermoelectric properties.

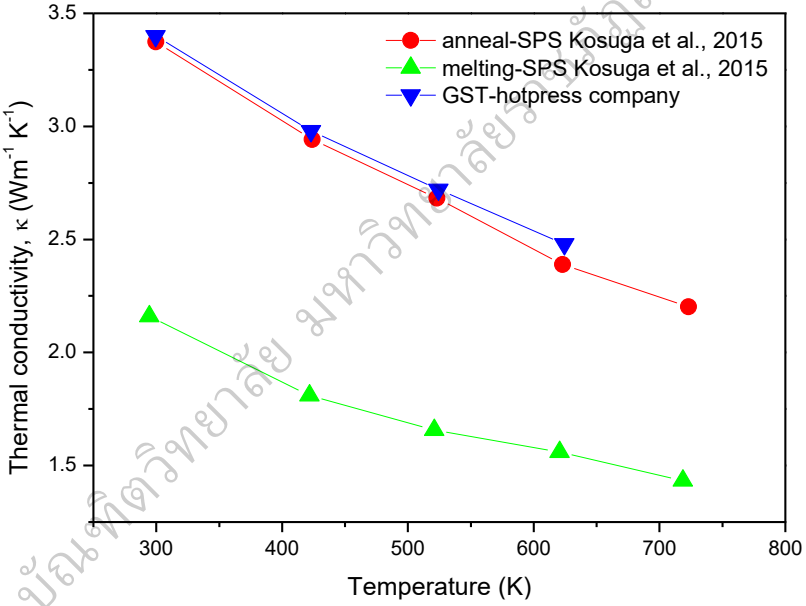

Figure 37 Temperature dependence of the thermal conductivity of GST-hotpress company sample compared with literature data [Kosuga *et al.*, 2015]

Dimensionless Figure of Merit

Figure 38 shows the temperature dependence of the dimensionless figure of merit, ZT . The ZT was calculated follow by equation:

$$ZT = \frac{S^2 \sigma T}{\kappa} \qquad (4\text{–}6)$$

Where S is the Seebeck coefficient, T is absolute temperature, σ the electrical conductivity, and κ the thermal conductivity. These results are of the fact that this sample exhibited Seebeck coefficient value, highest electrical conductivity and lowest thermal conductivity.

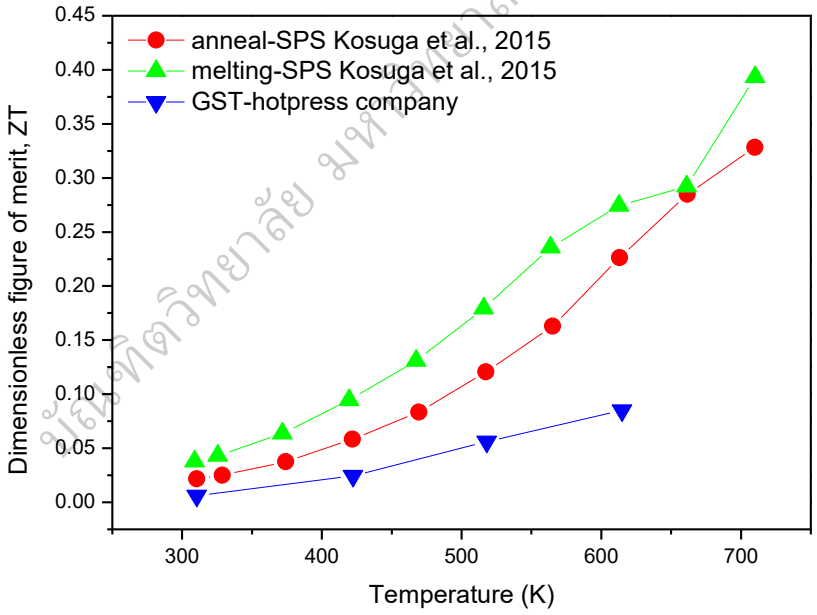

Figure 38 Show temperature dependence of the dimensionless figure of merit of GST–hotpress company sample compared with literature data [Kosuga *et al.*, 2015]

The ZT of GST-hotpress company sample was increased with increasing temperature but lower than that literature data over the whole temperature range. This is probably due to the variation of the synthesis methods employed, which lead to different material properties. In this study, we found that hot press had a little impact on the thermoelectric properties but it caused substantial changes in its crystal structure and element distribution.

Electronic Strucuture of GST-hotpress Sample

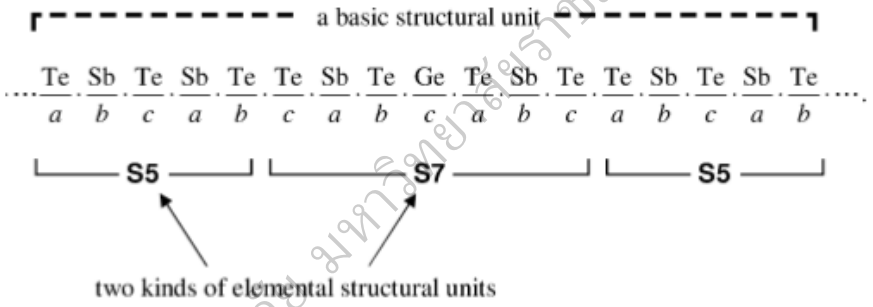

Figure 39 Show the structure of compound $GeSb_6Te_{10}$ is assumed to have the stacking (Shelimova, Karpinskii, Zemskov, & Konstantinov, 2000)

The GST materials has a rhombohedral structure mixture between $(GeTe)_n(Sb_2Te_3)_m$ homologous (HG) compounds. The GST materials are compound very narrow band gaps semiconductors in the energy range 0.20-2.80 eV and highly regarded as good performance TE materials. Firstly, we calculated thermoelelctric properties of GeTe and Sb_2Te_3 system using the density functional therory (DFT) and Boltzmann transport therory calculations based on QUANTUM ESPRESSO and BoltzTraP package (Andrea {Dal Corso} and Stefano de Gironcoli and Stefano Fabris and Guido Fratesi and

Ralph Gebauer and Uwe Gerstmann and Christos Gougoussis and Anton Kokalj and Michele Lazzeri and Layla Martin-Samos and Nicola Marzari and Francesco Mauri and Riccardo Mazzarello and Stefano Paolini and Alfredo Pasquarello and Lorenzo Paulatto and Carlo Sbraccia and Sandro Scandolo and Gabriele Sclauzero and Ari P Seitsonen and Alexander Smogunov and Paolo Umari and Renata M Wentzcovitch}, 2009). Secondly, we calculated the density of states (DOS) of GST-hotpress company sample compared with GeTe and Sb_2Te_3 from previous data. The DOS curve of $GeSb_6Te_{10}$ is relatively similar to that of Sb_2Te_3. We consider that this is a reasonable result taking into account the structural similarity of $GeSb_6Te_{10}$ and Sb_2Te_3. The $GeSb_6Te_{10}$ has six units of the Sb_2Te_3 layer and three units of the $GeSb_2Te_4$ layer in its structure. Because of the similarity with the $GeBi_2Te_4$ structure, as reported by (Kooi & De Hosson, 2002), the $GeSb_2Te_4$ structure can be considered to be the GeTe structure inserted in the middle of Sb_2Te_3 quintuple layers, that is, the structure of $GeSb_6Te_{10}$ is mainly composed of Sb_2Te_3. Therefore, the electronic structure of $GeSb_6Te_{10}$ would be more similar to that of Sb_2Te_3 than that of GeTe. The electronic band structure of $GeSb_6Te_{10}$ also shows a direct band gap at the Γ-point analogous to Sb_2Te_3. Moreover, the obtained band-gap energy (E_g) decreased with increasing Sb content: GeTe (0.98 eV) > $GeSb_6Te_{10}$ (0.52 eV) > Sb_2Te_3 (0.27 eV). A systematic study of the electronic band structures of GeTe-Sb_2Te_3 pseudobinary compounds, such as GeTe, $Ge_2Sb_2Te_5$, $Ge_1Sb_2Te_4$, $Ge_1Sb_4Te_7$, and Sb_2Te_3, using ab initio calculations has been reported (Park et al., 2009). It was found that the direct/indirect band gap and band-gap width depend on the composition. With increasing Sb content, the compounds change from indirect band gap to direct band gap compounds. GeTe, $Ge_2Sb_2Te_5$, and $Ge_1Sb_2Te_4$ have an indirect band gap, whereas $Ge_1Sb_4Te_7$ and Sb_2Te_3 have a direct band gap. Moreover, the band-gap energy decreases as the Sb content increases. Considering these results, our results are reasonable. We conclude that the

band structure of $GeSb_6Te_{10}$ has an indirect band gap, similar to Sb_2Te_3, but the band gap width is wider than that of Sb_2Te_3. Moreover, it is noteworthy that the slope of the DOS in the valence–band edge near the Fermi level of $GeSb_6Te_{10}$ is steeper than that of Sb_2Te_3, as shown in figure 40.

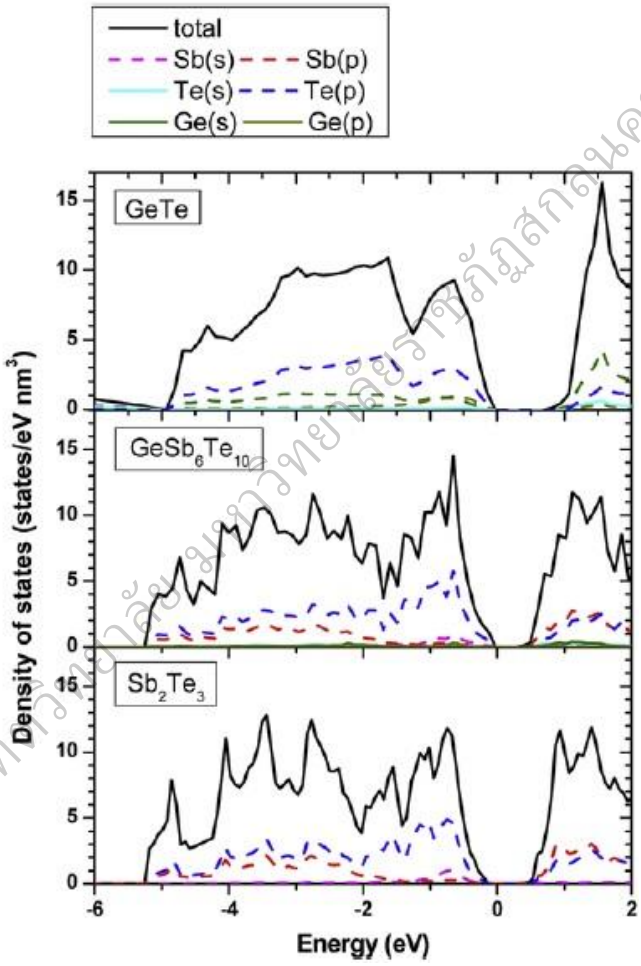

Figure 40 Shows orbital projected of density of states of GeTe, $GeSb_6Te_{10}$, and Sb_2Te_3

From these results of the above calculations part (Namhongsa et al., 2017), we can describe some basic features pf electronic structure of the $GeSb_6Te_{10}$ prepared by hot pressing method obtained in this study. The DOS of $GeSb_6Te_{10}$ is similar to those of

Matsunaga *et al.*, 2010 and Shelimova *et al.*, 2001, indicating that the samples are transition intermetallic with p–type conduction. This is consistent to the metallic behavior observed from the mechanical and electrical properties measurement.

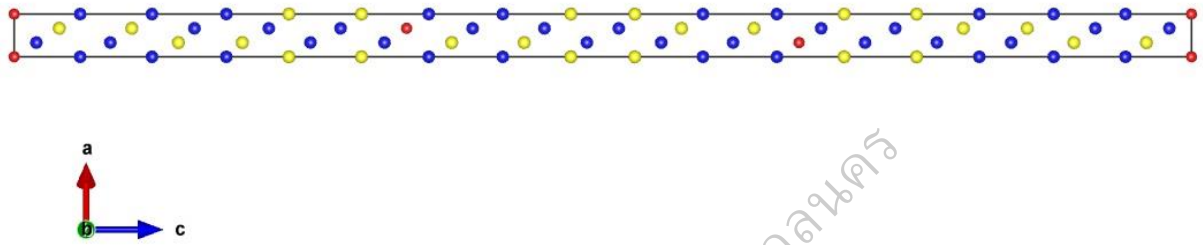

Figure 41 Show crystal structure of $GeSb_6Te_{10}$ with homologous structure consist $Ge_1Sb_2Te_4$–type slabs and Sb_2Te_3–types slabs, respectively.

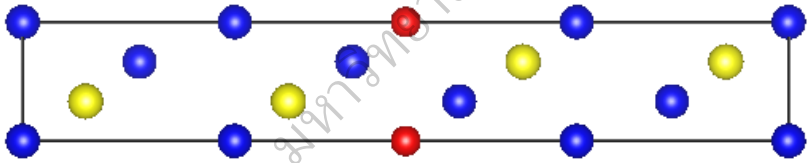

Figure 42 Show crystal structure of $Ge_1Sb_2Te_4$

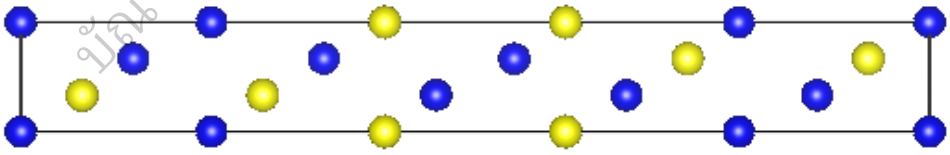

Figure 43 Show crystal structure of Sb_2Te

Thermoelectric Cell and Module

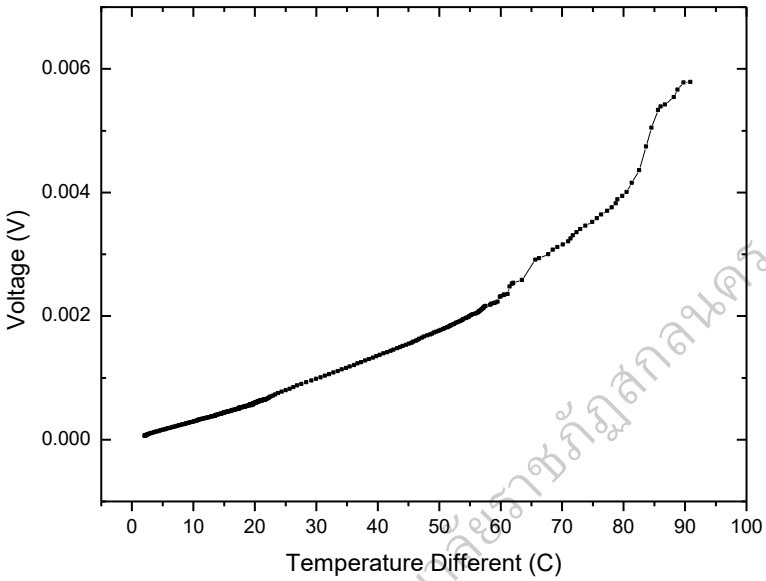

Figure 44 Show measured p–p junction 1 pair of GST thermoelectric cell

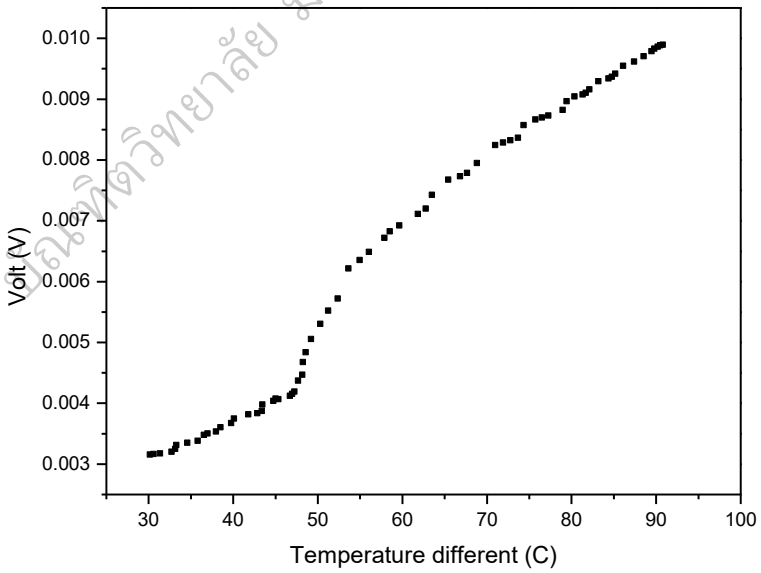

Figure 45 Show measured p–p junction 15 pairs of GST thermoelectric cell

Thermoelectric Application

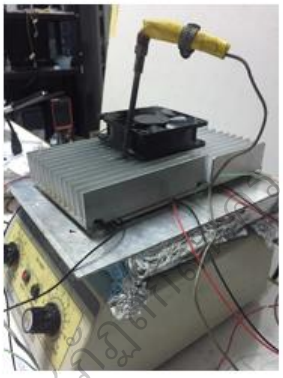

Figure 46 Show thermoelectric module from TEC Thermoelectric gencell technology and process of analyzed performance of 6–8 module by setting system on laboratory

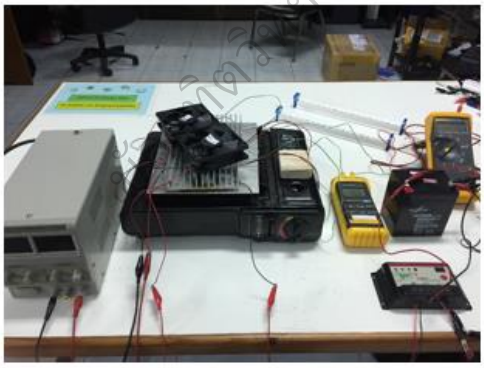

Figure 47 Shows system and how to measured electrical power of thermoelectric module for generate lighting system

Figure 48 Show thermogenerator machine for install on stove fuel of rice dryer Machine

In figure 46 and 47 shows how to measured electrical power of thermoelectric module from commercial. In firstly, we wanted to used thermoelectric module from GST-hotpress company sample for generate electricity on lighting system but after measured electrical power of GST-hotpress company module shows slightly values it not enough demand for used generate electricity on system. On system, we used 6-8 thermoelectric module from commercial and control hot side and cold side following by real temperature at Sri Sakon Pure-Rice Co.,Ltd.

Figure 48 show invention thermogenerator machine and building process for stick at stove fuel of rice dryer Machine. On the machine consist with thermoelectric module from commercial around 8 modules, four heatsinks and four ventilation fan stick on stainless steel wire. After install the machine on stove fuel of rice dryer Machine we checked system for generate electricity respectively.

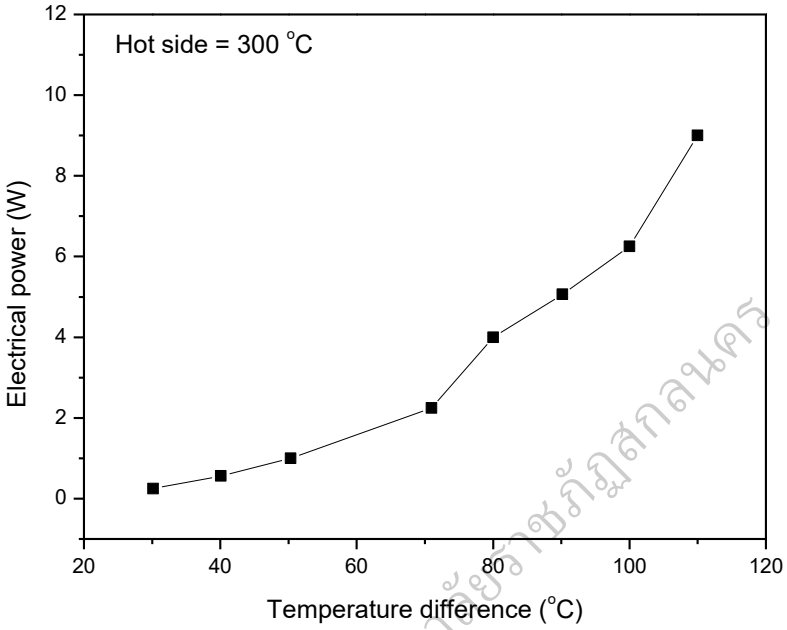

Figure 49 Show measured electrical power of 6-8 thermoelectric module from commercial for generating electricity for lighting system

From this figure 49 show electrical power value from thermoelectric module commercial has increased with increasing temperature. The highest value of electrical power is 9 Watt at temperature difference around 112 degree Celsius per 8 modules. The electrical power can be generate electricity for two light bulbs on these system.

References

Andrea {Dal Corso} and Stefano de Gironcoli and Stefano Fabris and Guido Fratesi and Ralph Gebauer and Uwe Gerstmann and Christos Gougoussis and Anton Kokalj and Michele Lazzeri and Layla Martin-Samos and Nicola Marzari and Francesco Mauri and Riccardo Mazzarello and Stefano Paolini and Alfredo Pasquarello and Lorenzo Paulatto and Carlo Sbraccia and Sandro Scandolo and Gabriele Sclauzero and Ari P Seitsonen and Alexander Smogunov and Paolo Umari and Renata M Wentzcovitch}, P. G. a. S. B. a. N. B. a. M. C. a. R. C. a. C. C. a. D. C. a. G. L. C. a. M. C. a. I. D. a. (2009). QUANTUM ESPRESSO: a modular and open-source software project for quantum simulations of materials. *Journal of Physics: Condensed Matter,, 21*, 395502 (395519pp).

Fan, X. A., Yang, J. Y., Chen, R. G., Yun, H. S., Zhu, W., Bao, S. Q., & Duan, X. K. (2006). Characterization and thermoelectric properties of p-type 25%Bi 2 Te 3 – 75%Sb 2 Te 3 prepared via mechanical alloying and plasma activated sintering. *Journal of Physics D: Applied Physics, 39*(4), 740.

Karpinsky, O. G., Shelimova, L. E., Kretova, M. A., & Fleurial, J. P. (1998). An X-ray study of the mixed-layered compounds of (GeTe)n (Sb2Te3)m homologous series. *Journal of Alloys and Compounds, 268*(1–2), 112–117. doi: http://dx.doi.org/10.1016/S0925-8388(97)00625-7

Kooi, B., & De Hosson, J. T. M. (2002). Electron diffraction and high-resolution transmission electron microscopy of the high temperature crystal structures of Ge x Sb 2 Te 3+ x (x= 1, 2, 3) phase change material. *Journal of applied physics, 92*(7), 3584-3590.

Kosuga, A., Nakai, K., Matsuzawa, M., Fujii, Y., Funahashi, R., Tachizawa, T., . . . Kifune, K. (2014). Enhanced thermoelectric performance of In-substituted GeSb6Te10 with

homologous structure. *APL Mater., 2*(8), 086102. doi: doi:http://dx.doi.org/10.1063/1.4893236

Kosuga, A., Nakai, K., Matsuzawa, M., Fujii, Y., Funahashi, R., Tachizawa, T., . . . Kifune, K. (2015). Crystal structure, microstructure, and thermoelectric properties of GeSb6Te10 prepared by spark plasma sintering. *Journal of Alloys and Compounds, 618*, 463–468. doi: http://dx.doi.org/10.1016/j.jallcom.2014.08.183

Lotgering, F. K. (1959). Topotactical reactions with ferrimagnetic oxides having hexagonal crystal structures—I. *Journal of Inorganic and Nuclear Chemistry, 9*(2), 113–123. doi: http://dx.doi.org/10.1016/0022-1902(59)80070-1

Matsunaga, T., Kojima, R., Yamada, N., Fujita, T., Kifune, K., Kubota, Y., & Takata, M. (2010). Structural investigation of GeSb6Te10 and GeBi6Te10 intermetallic compounds in the chalcogenide homologous series. *Acta Crystallographica Section B, 66*(4), 407–411. doi: doi:10.1107/S0108768110024080

Namhongsa, W., Omoto, T., Fujii, Y., Seetawan, T., & Kosuga, A. (2017). Effect of the crystal structure on the electronic structure and electrical properties of thermoelectric GeSb 6 Te 10 prepared by hot pressing. *Scripta Materialia, 133*, 96–100.

Park, J.-W., Eom, S. H., Lee, H., Da Silva, J. L., Kang, Y.-S., Lee, T.-Y., & Khang, Y. H. (2009). Optical properties of pseudobinary GeTe, Ge 2 Sb 2 Te 5, GeSb 2 Te 4, GeSb 4 Te 7, and Sb 2 Te 3 from ellipsometry and density functional theory. *Physical Review B, 80*(11), 115209.

Schneider, Matthias N., & Oeckler, O. (2010). GeSb4Te4 – a New 9P-Type Phase in the System Ge/Sb/Te *Zeitschrift für anorganische und allgemeine Chemie, 636*(1), 137–143. doi: 10.1002/zaac.200900453

Shelimova, L. E., Karpinskii, O. G., Zemskov, V. S., & Konstantinov, P. P. (2000). Structural and electrical properties of layered tetradymite-like compounds in the

GeTe—Bi2Te3 and GeTe—Sb2Te3 systems. *Inorganic Materials, 36*(3), 235–242. doi: 10.1007/BF02757928